

Comparative study of PVA/SiO₂ and PVA/SiO₂/glutaraldehyde (GA) nanocomposite membranes prepared by single-step solution casting method

Jagan Mohan Dodda¹ · Petr Bělský¹ · Josef Chmelář¹ · Tomáš Remiš¹ · Klára Smolná² · Martin Tomáš¹ · Lucie Kullová¹ · Jaroslav Kadlec¹

Received: 15 May 2015 / Accepted: 23 June 2015 / Published online: 1 July 2015
© Springer Science+Business Media New York 2015

Abstract We prepared poly(vinyl alcohol) (PVA)/SiO₂ and PVA/SiO₂/glutaraldehyde (GA) nanocomposite membranes in a single step using the solution casting method. The structure, morphology, and properties of these nanocomposite membranes were characterized by Raman spectroscopy, atomic force microscopy, small- and wide-angle X-ray scattering, thermogravimetric analysis, differential scanning calorimetry, and dynamic mechanical analysis (DMA). The influence of silica and GA loading on the meso-scale characteristics of the composite membranes was investigated. The results showed that silica deposited in the form of small nanoparticles (~1 nm) in the PVA/SiO₂ membranes, while bigger submicron particles (>25 nm) were formed in the PVA/SiO₂/GA membranes. The water uptake of the PVA/SiO₂ membranes increased with temperature, but the PVA/SiO₂/GA membranes were completely dissolved above 50 °C. We can therefore conclude that the addition of GA deteriorated the properties of PVA/SiO₂ membranes. The thermal stability of the PVA/SiO₂ membranes increased with the increasing silica loading with a maximum char yield of 46 % for PVA/SiO₂/4T. Even DMA profiles indicated a promising increase in E_R (rubbery modulus) from 6 MPa (PVA membrane) to 1015 MPa (PVA/SiO₂/4T) at 250 °C, showing high mechanical strength of these membranes.

Introduction

Hydrophilic PVA membranes are used in many applications, most notably in organic/inorganic separations, pervaporation, biomedical applications, catalysis, controlled drug release, etc. [1–4]. These membranes have a highly hydrophilic nature, which is considered as an advantage for some applications, but in most cases it becomes a hindrance due to the high swelling capacity of the membranes in water. To enhance the stability and performance of PVA-based membranes, a variety of chemical modifications have been employed, e.g., cross-linking [5–7], electrospinning [8–10], blending [11], sol–gel process [12, 13], and grafting [14, 15].

Cross-linking is considered as a suitable way to alter the physical and chemical properties of membranes. The polyhydroxy structure of PVA enables easy cross-linking with various multifunctional compounds capable of reacting with –OH groups to obtain *three-dimensional* networks. A majority of the commercially available asymmetric PVA membranes are cross-linked by the phase-inversion technique [16, 17]. Recently, M'barki et al. [18] proposed a unique greener method to prepare porous polymer membranes by combining thermally induced phase separation and cross-linking of PVA in water. Their results showed that cross-linking control was the key step to obtain a porous membrane morphology. A different approach was followed by Casimiro et al. [19], who prepared PVA-supported catalytic membranes for biodiesel production by the mutual γ -irradiation method. They used adipic acid (AA) and succinic acid (SA) as crosslinkers and a commercial ion-exchange resin as the catalyst. The results showed that a slight increase in the γ -radiation dose leads to an increase of the membrane catalytic activity.

Currently, most of the membrane studies are focused towards easy fabrication of composite membranes in a single step using methods such as surface segregation [20,

✉ Jagan Mohan Dodda
jagan@ntc.zcu.cz

¹ New Technologies – Research Centre, University of West Bohemia, Univerzitní 8, 306 14 Plzeň, Czech Republic

² Department of Chemical Engineering, University of Chemistry and Technology, Technická 5, 166 28 Prague 6, Czech Republic

21], solution casting [22–24], or dip-coating [25, 26]. In the literature, many kinds of PVA-based hybrid membranes using silica constituents were reported [27–29], but the solution casting method is rarely used for directly fabricating PVA/SiO₂ membranes. In this method, the preparation of membranes becomes challenging for many reasons, for example, solidification of the casting solution, gel formation after using the cross-linking agent, stiffness due to SiO₂ loading, etc. Therefore, optimum conditions have to be maintained to synthesize this kind of composite membranes with good mechanical and thermal stabilities.

In this work, we develop a single-step solution casting method for the preparation of PVA/SiO₂ and PVA/SiO₂/GA nanocomposite membranes. Our idea was to incorporate silica and GA directly into the PVA matrix in a simple way, which can be economically viable. Therefore, the PVA/SiO₂ membranes were synthesized by direct addition of TEOS and HCl to the PVA casting solution, while the PVA/SiO₂/GA membranes were prepared by further adding GA to the PVA–TEOS solution. Membranes with different contents of silica and GA were characterized by Raman spectroscopy, small- and wide-angle X-ray scattering (SAXS/WAXS), atomic force microscopy (AFM), thermogravimetric analysis (TGA), differential scanning calorimetry (DSC), dynamic mechanical analysis (DMA), and water uptake experiments. The effect of silica and GA incorporation on the properties and morphology of the nanocomposite membranes was systematically investigated.

Materials and methods

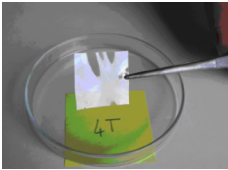
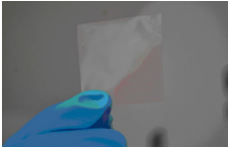
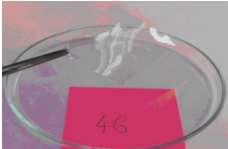
Materials

PVA (hydrolyzed 99+%, $M_w = 86000$ – 98000) and GA (25 % in water) were obtained from Sigma-Aldrich (USA). TEOS and hydrochloric acid (HCl, 37 wt%) were purchased from Merck Chemicals (Germany). All the chemicals were of analytical grade and used as received. Deionized water was utilized for all the membrane preparation experiments.

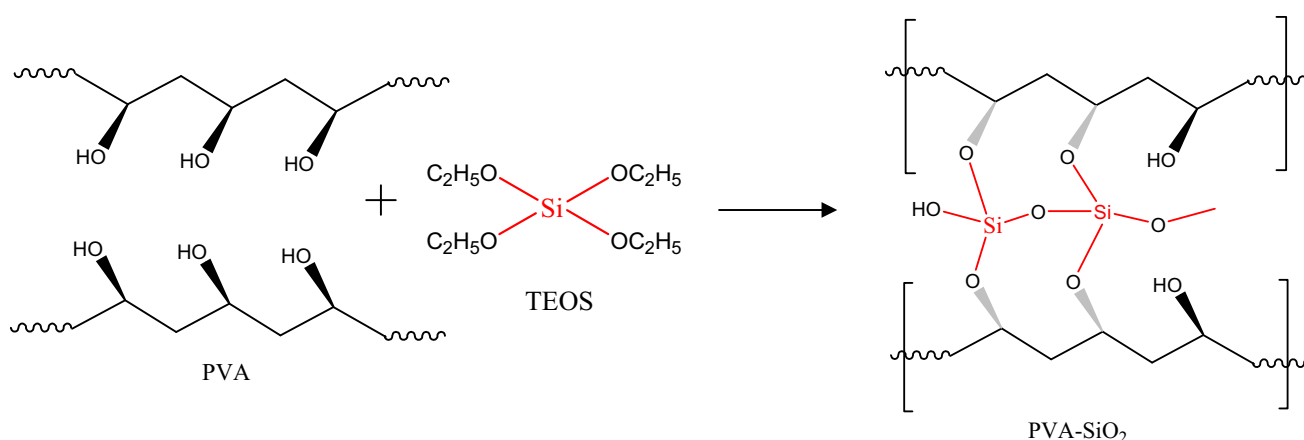
Membrane preparation

Nanocomposite PVA membranes were prepared by the solution casting method. At first, a 5 wt% solution of PVA in water was prepared by continuous stirring at 90 °C until the complete dissolution was achieved. Subsequently, TEOS, HCl, and GA were directly added to the PVA solution at room temperature and the stirring was continued for 4 h. The composition of each solution is specified in Table 1. The prepared solution was poured into the automatic film applicator (TQC, Germany) equipped with a glass plate and was fabricated into membranes with uniform thickness. The expected reactions and membrane structures are shown in Schemes 1 and 2.

Table 1 Composition of solutions for the composite membranes

Membrane code	Composition ^a	Membranes
PVA/SiO ₂ /1T	1 ml TEOS + 0.5 ml HCl	 PVA/SiO ₂ /4T
PVA/SiO ₂ /2T	2 ml TEOS + 0.5 ml HCl	
PVA/SiO ₂ /3T	3 ml TEOS + 0.5 ml HCl	
PVA/SiO ₂ /4T	4 ml TEOS + 0.5 ml HCl	
PVA/SiO ₂ /GA1	1 ml TEOS + 0.5 ml HCl + 1 ml GA	 PVA/SiO ₂ /GA4
PVA/SiO ₂ /GA2	1 ml TEOS + 0.5 ml HCl + 2 ml GA	
PVA/SiO ₂ /GA3	1 ml TEOS + 0.5 ml HCl + 3 ml GA	
PVA/SiO ₂ /GA4	1 ml TEOS + 0.5 ml HCl + 4 ml GA	
PVA/GA1	1 ml GA	 PVA/GA4
PVA/GA2	2 ml GA	
PVA/GA3	3 ml GA	
PVA/GA4	4 ml GA	

^a Solution mixtures were added to 5 % PVA (100 ml) solution



Scheme 1 Expected chemical reactions during the formation of the PVA/SiO₂ membranes

Characterization

Raman spectroscopy

The Raman measurements were carried out on a DXR Raman microscope (Thermo Scientific, USA). Three excitation lasers (532, 633, and 780 nm) and four apertures (slit and pinhole, 25 and 50 μm) were tested. The best results were obtained using the 532 nm laser with the 50- μm pinhole aperture. This configuration was thus used for all measurements. The laser power was set to 10 mW and 1000 scans with a 1-s exposure time were recorded for each spectrum. To check sample homogeneity and eliminate any possible artifacts, at least four spectra at different points were collected for each sample. Since the bands relevant to this study are in the range from approximately 800–1700 cm^{-1} , we used the high-resolution grating for all experiments. This grating provides the spectral resolution of 2 cm^{-1} in the range from 70 to 1870 cm^{-1} . The band at 855 cm^{-1} was not influenced by adding TEOS or GA [30] and was therefore used for the intensity normalization of the Raman spectra, when required for evaluation purposes.

Small- and wide-angle X-ray scattering

The SAXS/WAXS experiments were performed on a SAXSess mc^2 instrument (Anton Paar, Austria). The instrument uses a GeniX Microfocus X-ray point source with a Cu anode (50 kV and 1 mA), single-bounce focusing X-ray optics, and an advanced collimation block. This configuration enables to measure in point collimation geometry only. The experiments were performed in the standard transmission setup, and imaging plates together with the CyclonePlus[®] Reader (PerkinElmer, Inc.) were used for detection. The sample exposure time was 30 min and four pieces of the membranes were stacked for each measurement. The range of the scattering vector magnitude

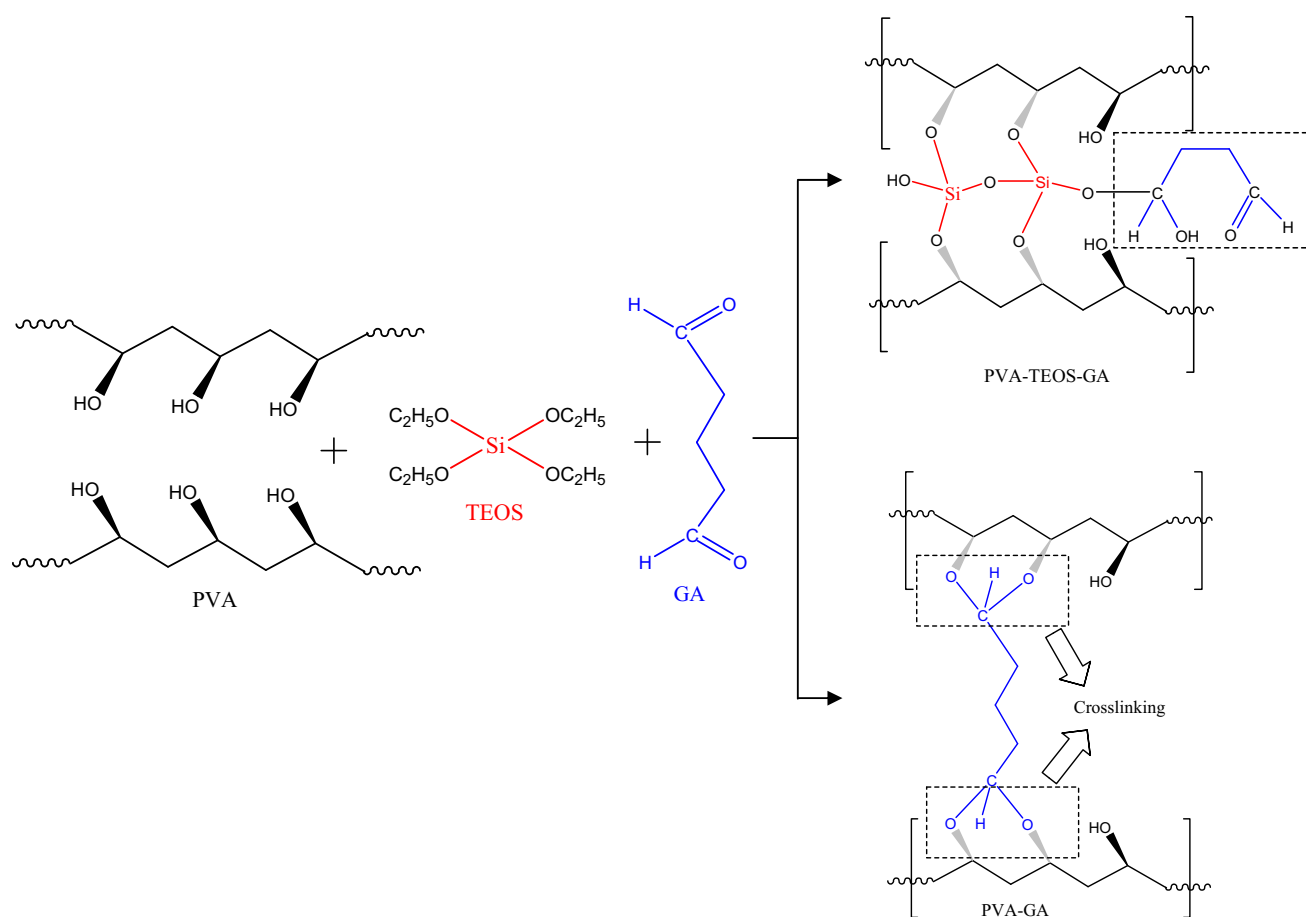
for the used experimental setup starts at about 0.2 nm^{-1} and goes up to 28 nm^{-1} . It therefore covers both the SAXS and the WAXS range. The scattering vector magnitude q is defined as $q = (4\pi/\lambda) \sin\theta$, where λ is the X-ray wavelength (0.15418 nm for Cu K α) and θ is the half-scattering angle (Bragg angle). The 1D radial intensity profiles were created from the measured 2D patterns by azimuthal averaging using the SAXSquant software (Anton Paar, Austria), which could be performed thanks to the azimuthal symmetry of these patterns (indicating the isotropic nature of the investigated samples).

Atomic force microscopy

The morphological measurements were conducted on the atomic force microscope Ntegra (NT-MDT, Russia) in the semi-contact mode. Several semi-contact probes were tested and the probe HA-NC (also NT-MDT) with a force constant of 3.5 N/m was chosen as the most suitable for the morphological mapping of prepared PVA membranes. The typical scanning frequency was 0.6 Hz and the free oscillating amplitude (FOA) was 1.8 V. The set point amplitude (SPA) was individually chosen for each sample to the value of SPA = 0.5·FOA. The NT-MDT software allows the scanning of four images during one AFM scan. We scanned two topological images (trace and retrace), one phase image and one magnitude image. The magnitude image was recorded for each measurement and helped in non-ambiguous image interpretations. A comparison of the trace and retrace images allows in excluding artifacts which could be created by wrong SPA.

Water uptake measurements

The water uptake studies were carried out at temperatures from 30 to 90 $^{\circ}\text{C}$ with a 20 $^{\circ}\text{C}$ step. The membranes were placed in deionized water, heated to 30 $^{\circ}\text{C}$ and kept at this



Scheme 2 Expected chemical reactions during the formation of PVA/SiO₂/GA membranes

temperature for 1 h at ambient pressure. The wet membranes were then wiped with a filter paper and weighted. Temperature was then increased by 20 °C and the whole process was repeated until the data were acquired at all desired temperatures.

Thermogravimetric analysis

Dynamic TG analyses were performed to assess the relative thermal stabilities of the polymer membranes. The TGA curves were obtained on a TGA Q500 thermogravimetric analyzer (TA Instruments, USA). Samples of about 5 mg were heated at a rate of 10 °C/min in N₂ atmosphere. The weight of the samples was measured as a function of temperature/time.

Differential scanning calorimetry

A DSC Q200 differential scanning calorimeter (TA Instruments, USA) was used to measure the phase transition behavior of the membranes. Samples of about 5 mg were weighed into a DSC aluminum pan. Dynamic heating

scans were carried out from 50 to 300 °C at a heating rate of 10 °C/min in N₂ atmosphere.

Dynamic mechanical analysis

The temperature dependence of the storage modulus was determined by DMA using a DMA Q800 instrument (TA Instruments, USA). Membrane samples with a size of 13 × 0.8 mm and a thickness of about 1 mm were used to measure the mechanical properties. Experiments were conducted in N₂ atmosphere at three different frequencies (1, 10 and 20 Hz) starting from ambient temperature up to 250 °C with a heating rate of 5 °C/min.

Results and discussion

Raman spectroscopy

The Raman spectra of the pure PVA, PVA/SiO₂, and PVA/SiO₂/GA membranes were measured and the assignment of the major Raman bands is summarized in Table 2. In the

Table 2 Assignment of Raman bands for PVA, PVA/SiO₂, and PVA/SiO₂/GA membranes

Frequency (cm ⁻¹)	Assignment
856	C–C stretching [31, 33, 34]
919	C–C stretching [30, 31, 33, 34]; increase in the intensity can be related to the decrease of the crystallinity, i.e., represents non-crystalline conformation of the PVA carbon backbone
980	Si–OH stretch [31, 32]
1071	C–O stretching, O–H bending [30, 31]
1093	C–O stretching, O–H bending [30, 31, 33]
1124	very weak in this spectrum; C–O and C–C stretching [31]; C–O–C stretching in the cross-linked network [30]; indicative of the amorphous phase [30, 31]
1147	C–O and C–C stretching [30, 31, 33]; indicative of the crystalline phase [30, 31, 34]
1365	C–H and O–H bending [30, 31, 34]
1442	C–H and O–H bending [30, 31, 33, 34]

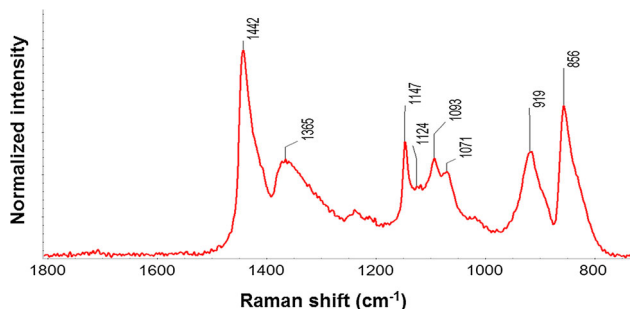


Fig. 1 Raman spectrum of pure PVA

pure PVA membrane spectrum (Fig. 1), strong characteristic bands were observed at 856, 919, 1147, and 1442 cm⁻¹. The bands at 856 and 919 cm⁻¹ are due to the C–C stretching of the PVA polymer backbone. The band at 919 cm⁻¹ corresponds to the amorphous phase (non-crystalline conformation of the PVA carbon backbone), while the band at 856 cm⁻¹ is independent of the crystallinity [30] and was therefore used for intensity normalization, as mentioned in the experimental section. The bands at 1365 and 1442 cm⁻¹ result from the C–H and O–H bending vibrations and the bands at 1147 and 1124 cm⁻¹ correspond to the C–C and C–O stretching in the crystalline and the amorphous phase of the PVA matrix, respectively.

The spectra of the pure PVA, PVA/SiO₂/2T, and PVA/SiO₂/4T membranes are compared in Fig. 2a. It is clearly visible that the incorporation of silica reduced the crystallinity of the membranes. The “crystalline” band at 1147 cm⁻¹ decreased and the “amorphous” band at 1118 cm⁻¹ increased with the increasing silica loading. The intensity ratio of the bands at 916 and 856 cm⁻¹ increased with the increasing SiO₂ content, also indicating

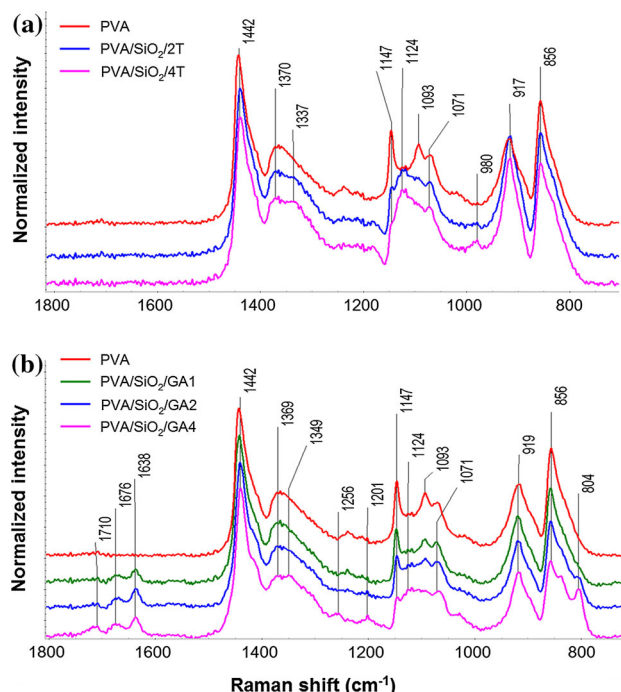


Fig. 2 Comparison of Raman spectra of PVA and a PVA/SiO₂; b PVA/SiO₂/GA membranes

a decrease of the crystallinity. A new feature in the spectrum is the weak scattering band at 980 cm⁻¹ corresponding to Si–OH vibrations [31, 32]. A significant shoulder appears around 1337 cm⁻¹ for PVA/SiO₂/2T and then forms a second maximum for PVA/SiO₂/4T. The same trend was observed by Martinelli et al. [30] for PVA membranes with various contents of GA and silica. The band at 1094 cm⁻¹ completely disappeared upon the addition of TEOS. Since this band is related to O–H vibrations, this could be evidence that the OH groups in PVA reacted with TEOS. The small band that would represent unreacted OH groups is probably overlapped by the neighbouring strong and broad band at 1118 cm⁻¹.

The spectra of samples PVA/SiO₂/GA1, PVA/SiO₂/GA2, and PVA/SiO₂/GA4 are compared with that of pure PVA in Fig. 2b. The intensity of the band at 1147 cm⁻¹ decreased with the increasing GA content and, simultaneously, a slight increase in the 1118 cm⁻¹ band intensity was observed, clearly indicating a decrease of the membrane crystallinity. However, the decrease of the crystallinity was gradual in the case of PVA/SiO₂/GA membranes, in contrast with the PVA/SiO₂ samples.

The addition of GA resulted in the emergence of several new bands, especially at the highest GA content (sample PVA/SiO₂/GA4). These bands were at 1710, 1676, 1638, 1256, 1201, and 804 cm⁻¹, respectively, and can be attributed to various vibrations in pure GA [30]. Martinelli et al. [30] measured the Raman spectra of PVA cross-linked by various amounts of GA and suggested that only a

limited amount of GA was incorporated into the PVA network. We would therefore suggest that the observed bands originate from GA molecules that did not fully incorporate into the cross-linked network. This is supported by the fact that the intensity of these bands increased with the increasing GA content, in agreement with [30]. Furthermore, several of these bands (1710, 1256, 1201, and 804 cm^{-1}) were not observed at the lowest GA content (PVA/SiO₂/GA1), supporting the assumption that a small amount of GA incorporates into the membrane. The band at 1369 cm^{-1} broadens to lower wavenumbers, although this effect is less notable for PVA/SiO₂/GA than for the corresponding PVA/SiO₂ membranes, probably indicating a lower incorporation of silica into the membrane structure when GA is present. This assumption was confirmed by SAXS.

Small- and wide-angle X-ray scattering

Figure 3a–c show the SAXS profiles of the PVA/SiO₂, PVA/SiO₂/GA, and PVA/GA samples, respectively. The profile of pure PVA is shown in all cases for comparison. The profiles are expressed as dependencies of the scattering intensity on the scattering vector magnitude q on a log–log scale. The corresponding WAXS profiles are shown in Fig. 4a–c and expressed as dependencies of the scattering/diffraction intensity on the 2θ angle.

The WAXS profile of the pure PVA membrane shows several crystalline peaks that could be well assigned to crystallographic planes of the monoclinic PVA system [35, 36]. The crystalline peaks are superimposed on a broad amorphous halo corresponding to the amorphous phase. Thus, the WAXS profile verified the semi-crystalline nature of the pure PVA membrane.

The nanometer-scale structure can be estimated from the SAXS profile. The peak in the SAXS profile of the pure PVA membrane at q of approximately 0.6 nm^{-1} is an evidence for the nanophase separation of the material, i.e., mixed crystalline and amorphous regions with dimensions in the range of nanometers, in accordance with the literature [37]. The corresponding approximate d -spacing calculated from the position of the peak maximum is: $d = 2\pi/q_{\text{max}} = 2\pi/0.7 = 9\text{ nm}$. The pronounced peak shows that the structure is well ordered with a relatively narrow distribution of both the size of the crystallites and their spacing. If we assume small crystallites randomly distributed in an amorphous polymer matrix [37], their size and average distance can be estimated from the SAXS profile. For this purpose, we utilized the *Irena* software package for small-angle scattering analysis [38]. If the crystallites are assumed to be spherical, the SAXS profile fitting provides an average diameter of about 6 nm with an average d -spacing of about 8 nm.

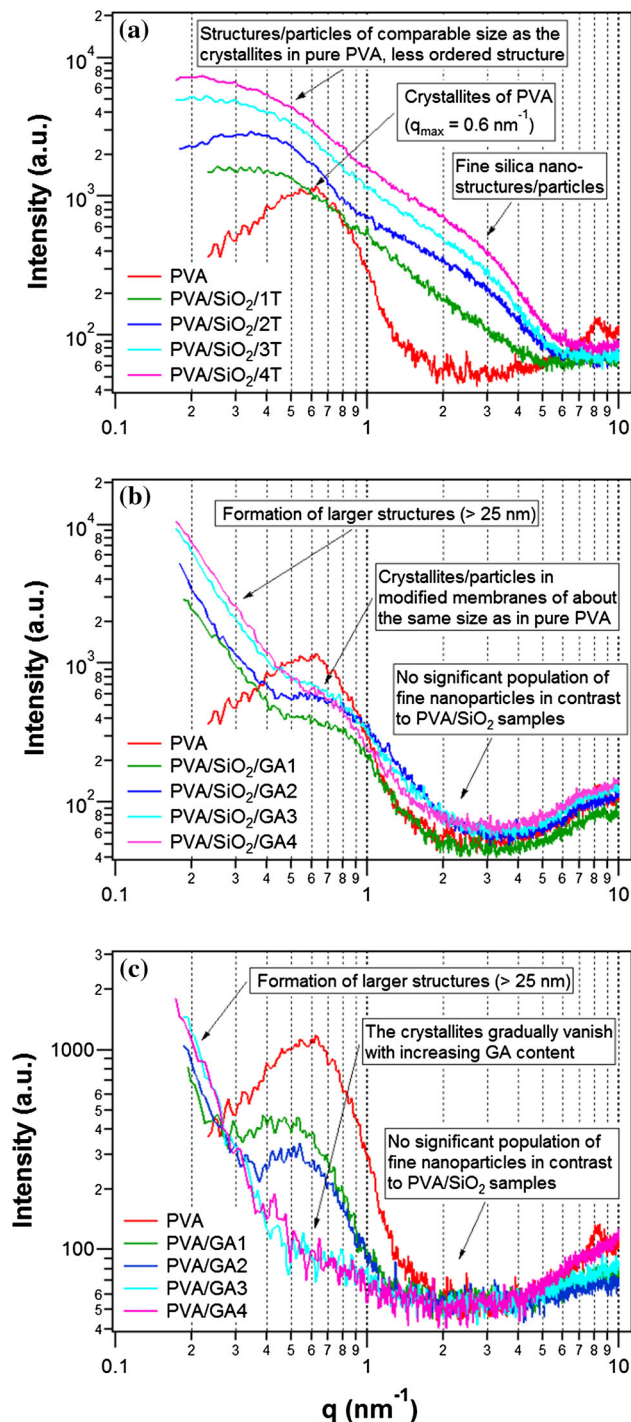


Fig. 3 SAXS profiles of **a** PVA/SiO₂, **b** PVA/SiO₂/GA, and **c** PVA/GA membranes

With the increasing silica (TEOS) loading, the crystalline peaks decrease in intensity or vanish (Fig. 4a), indicating a decrease in the crystallinity of the membranes. For PVA/SiO₂/3T and PVA/SiO₂/4T, all peaks corresponding to crystalline PVA virtually vanished. This observation correlates very well with the results of Raman spectroscopy. The SAXS profiles of the PVA/SiO₂ samples

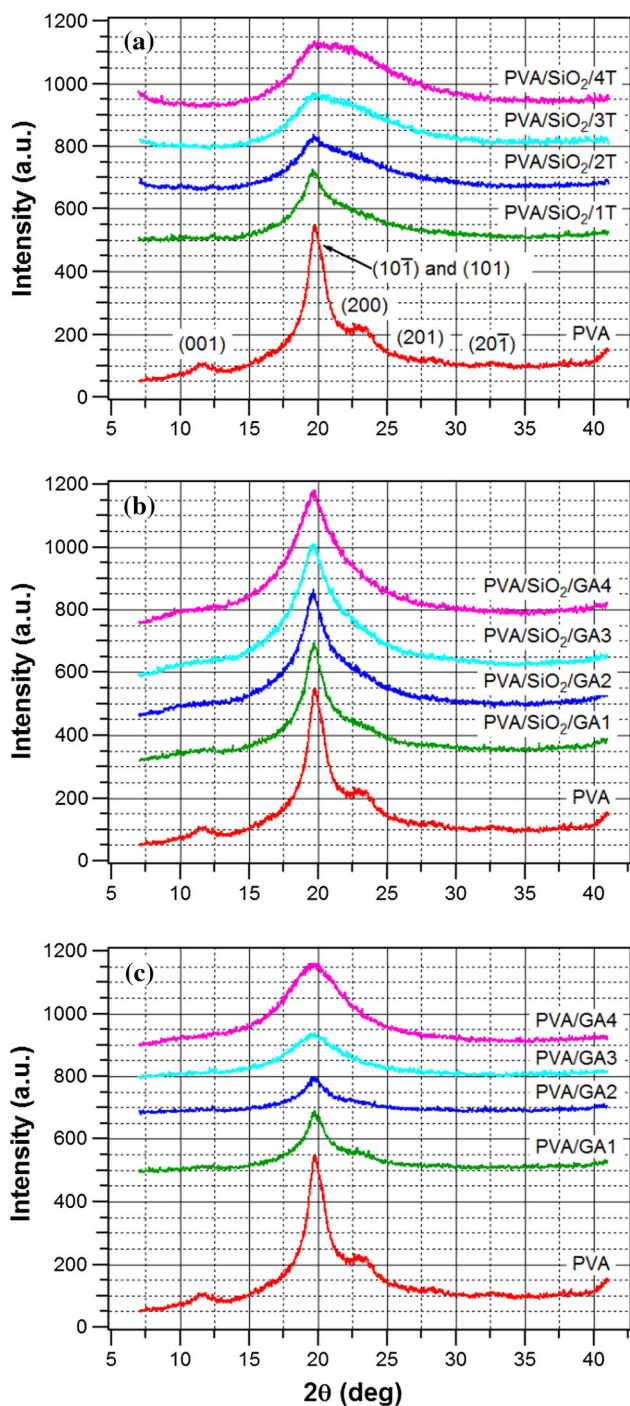


Fig. 4 WAXS profiles of **a** PVA/SiO₂, **b** PVA/SiO₂/GA, and **c** PVA/GA membranes

provide further information. First, the fact that the peak of PVA did not vanish indicates that there still exists phase separation on the nanometer scale with similar dimensions as in the pure PVA structure. However, we can hardly talk about semi-crystalline structure because, as discussed above, the crystallinity of the PVA/SiO₂ membranes decreased or virtually vanished with the increasing silica

loading. With the increasing SiO₂ loading, the peak of PVA becomes broader and shifts to lower values of *q*, which indicates that the structure is less ordered than that of the pure PVA membrane, presumably with a wider distribution of the particle sizes. The shift of the peak position to lower values of *q* does not necessarily mean that the average *d*-spacing grows, but it can also be caused just by the less sharp structure factor profile due to the less ordered structure. The new broad shoulder at higher scattering vectors, which is not present in pure PVA, indicates the presence of fine nanoparticles/nanostructures (with dimensions down to about 1 nm), which must be silica or silica-containing particles/structures distributed in the polymer matrix. The above observations are clear evidence that silica is extensively incorporated into the PVA structure. Furthermore, a successful formation of organic–inorganic composites of PVA and silica was already reported and studied by SAXS and FTIR in [39], where the same reaction of PVA with TEOS was used for the composite preparation.

Figure 4b shows the WAXS profiles of the PVA/SiO₂/GA samples. It can be seen that when TEOS and GA are added, the intensity of the crystalline peaks decreases, as in the previous case. However, the influence of increasing the GA concentration on the crystallinity is not that strong as in the case of TEOS, in a good agreement with the results of Raman spectroscopy. Figure 3b shows the SAXS profiles of the PVA/SiO₂/GA membranes. In this case, the situation is completely different compared to the PVA/SiO₂ membranes. The peak corresponding to the PVA crystallites does not shift, which means that their size is preserved. No significant shoulder at higher scattering vector *q* is present, which means that silica does not incorporate into the polymer in the form of fine nanoparticles. The steep rise of the scattering intensity towards low *q* originates from the presence of bigger particles (at least 25 nm). Such particles did not form in the PVA/SiO₂ membranes. Thus, in the case of PVA/SiO₂/GA membranes, silica prefers to form bigger particles, presumably together with GA. This correlates very well with the TGA results, which showed that the PVA/SiO₂/GA membranes are less stable than the PVA/SiO₂ membranes and that their thermal stability did not even increase in comparison with the pure PVA membranes. These findings correspond very well with the AFM results, which showed the presence of such big particles in the PVA/SiO₂/GA samples, whereas the morphology of PVA/SiO₂ was similar to that of pure PVA.

Figures 3c and 4c show the SAXS and WAXS profiles of the PVA/GA samples, which were additionally prepared for selected supplementary analyses. It can be observed from the SAXS profiles that the addition of GA leads to a gradual decrease of the peak corresponding to the nanocrystallites. In the case of PVA/GA3 and PVA/GA4,

the peak totally vanished. The WAXS profiles of the PVA/GA samples (Fig. 4c) confirm the decrease in crystallinity with the increasing GA content. It can therefore be concluded that a sufficiently high concentration of GA prevents the formation of the fine semi-crystalline structure. This indicates that GA effectively reacts with the hydroxyl groups of PVA and cross-links the PVA chains when the GA concentration is sufficiently high. The GA side chains and cross-links then prevent the formation of the nanocrystallites, which form in pure PVA. This is a different situation compared with the PVA/SiO₂/GA samples, where the SAXS peak did not vanish even at the highest GA concentration (only its intensity was reduced). Simultaneously, the crystallinity determined by WAXS did not decrease that intensely as in the case of the corresponding PVA/GA samples. These observations further support the conclusion that GA preferably reacts with TEOS (silica) and not with PVA. Therefore, it can be concluded that GA is not a suitable cross-linking agent of PVA in the presence of TEOS and that the cross-linking is significantly more effective when TEOS is not present.

The steep rise of the SAXS profiles (Fig. 3c) towards low q values indicates the formation of bigger domains (at least 25 nm) in the PVA/GA membranes (same as in the case of the PVA/SiO₂/GA samples). These domains are formed either by unreacted free GA or some ordered structures on larger scale due to the effective GA cross-linking.

Atomic force microscopy

The morphology of the pure PVA membrane and the composite PVA/SiO₂/4T and PVA/SiO₂/GA3 membranes was studied by AFM and is presented in Figs. 5, 6, and 7. The surface of pure PVA on the microscale is finely homogeneous, as seen in Fig. 5a. The closely packed semi-crystalline PVA structure is shown in Fig. 5b on a finer scale, although the fine nanometer structure is beyond the resolution capabilities of the instrument due to the size of the AFM tip which is at least 10 nm.

At the microscale, the PVA/SiO₂/4T membrane showed a homogeneous morphology (Fig. 6a), which is very similar to that of the pure PVA membrane (Fig. 5a). At the finer scale, the morphology of the composite membrane (Fig. 6b) showed to be smoother than that of the pure PVA membrane (Fig. 5b). This can also be clearly observed by comparing the z-axis of the AFM images in Figs. 5 and 6. The given conclusions are in a very good agreement with the SAXS analysis, which showed the presence of fine nanometric particles in the PVA/SiO₂ composite membranes and no formation of bigger particles.

On the other hand, the surface of the PVA/SiO₂/GA3 sample showed large domains with a relatively broad size distribution (from tens to hundreds of nanometers), see Fig. 7. This confirms the presence of large particles, which were also observed by SAXS for all PVA/SiO₂/GA samples. These particles are formed by GA and silica that did not get incorporated into the polymer.

Water uptake

The water uptake (W_u) was calculated using the following equation:

$$W_u = \frac{W_s - W_d}{W_d},$$

where W_s and W_d are the weights of swollen and dry membranes, respectively.

Figure 8 shows the effect of temperature on the water uptake properties of the PVA/SiO₂ membranes. Recently, Xie et al. [40] reported a significant decrease in the water uptake of PVA/MA/TEOS hybrid membranes from 154 to 43 % when the temperature was raised from 21 to 100 °C. However, our PVA/SiO₂ membranes have shown a gradual increase in W_u with the increasing temperature, as shown in Fig. 8. The W_u values ranged from 16–20 % at 30 °C to 60–117 % at 90 °C. For example, PVA/SiO₂/3T showed an increase of the water uptake from 18 to 117 % when the membrane was heated from 30 to 90 °C. The PVA/SiO₂ membranes show a good balance between the hydrophilicity and the thermal stability, as will be demonstrated in the TGA section. On the other hand, the PVA/SiO₂/GA membranes were completely dissolved when the temperature was raised above 50 °C. This corresponds well with the fact that the molecular structure of the PVA/SiO₂/GA membranes is not effectively reinforced and that their thermal and mechanical stability is relatively poor. It was shown that the binding of PVA with TEOS and GA was not effective enough to form a stable structure, which caused an increase in hydrophilicity, but reduced the thermal stability. The excess hydrophilic nature of the PVA/SiO₂/GA membranes resulted in the dissolution of the membranes at higher temperatures.

Thermal analysis

The thermal degradation of pure PVA membranes showed two distinct steps in the TGA curve (Fig. 9). The first step occurred between 200 and 330 °C (with a sharp decrease around 260 °C) with a major weight loss of 69 %. The second step followed between 330 and 520 °C with a weight loss of ~15 %. Previous studies have shown that the decomposition of PVA begins with chain “stripping”,

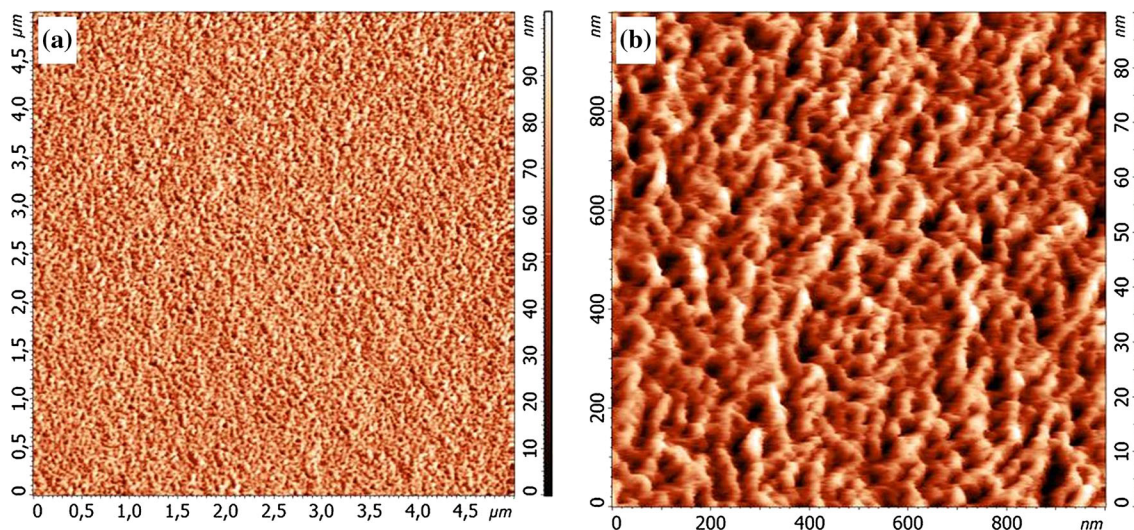


Fig. 5 AFM topological images of PVA membrane on **a** micron and **b** submicron scale

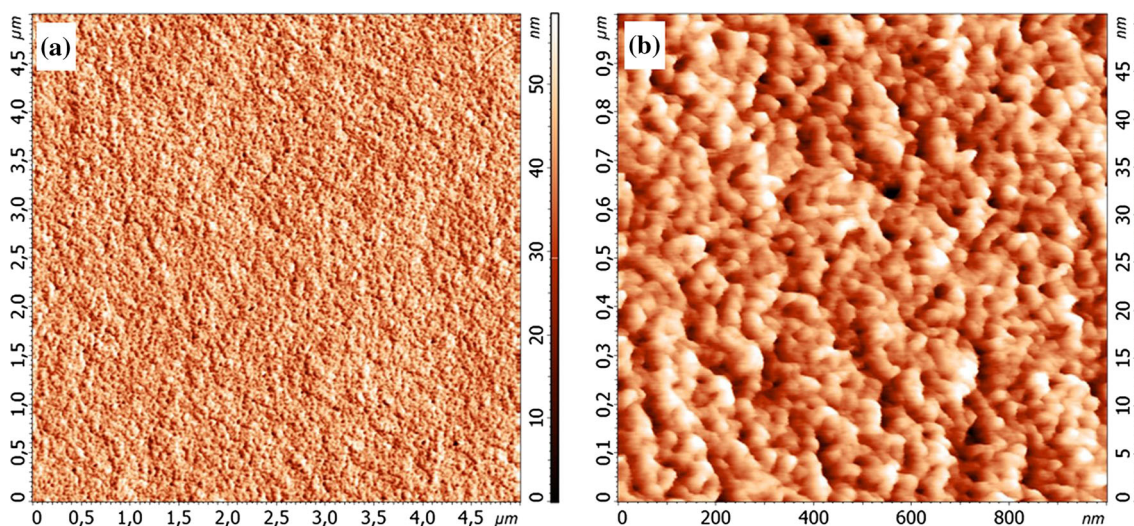


Fig. 6 AFM topological images of PVA/SiO₂/4T membranes on **a** micron and **b** submicron scale

i.e., the elimination of water accompanied by the formation of polyene structures, as shown in Fig. 9. At higher temperatures (>350 °C), these polyene structures are further converted to low-molecular weight aliphatic products [41–43].

The presence of silica in the PVA matrix improved the thermal stability of the PVA/SiO₂ membranes (Fig. 10a). Furthermore, the distinct two-step degradation pattern of pure PVA did not occur in this case. Instead, a slow and gradual degradation pattern was observed for the PVA/SiO₂ membranes, which was due to their less ordered, predominantly amorphous structure. Although it is difficult to define a clear initial decomposition temperature from the TGA curves due to the continuous weight loss, it was still

possible to distinguish two weight loss stages. The first stage occurred in the temperature range from 50 to about 450 °C with the maximum weight loss of ~70 % observed for PVA/SiO₂/1T and the minimum weight loss of ~35 % for PVA/SiO₂/4T. For the 2T, 3T, and 4T samples, the first stage continuously passed into the second stage corresponding to the chain degradation. The char yield values of the PVA/SiO₂ membranes increased with the increasing silica loading, with the maximum char yield of 46 % observed for the PVA/SiO₂/4T membrane.

The earlier onset of the weight loss of samples 2T, 3T, and 4T in comparison with pure PVA suggests that the chain stripping process starts at a lower temperature, which means that at the beginning, water can cleave off more

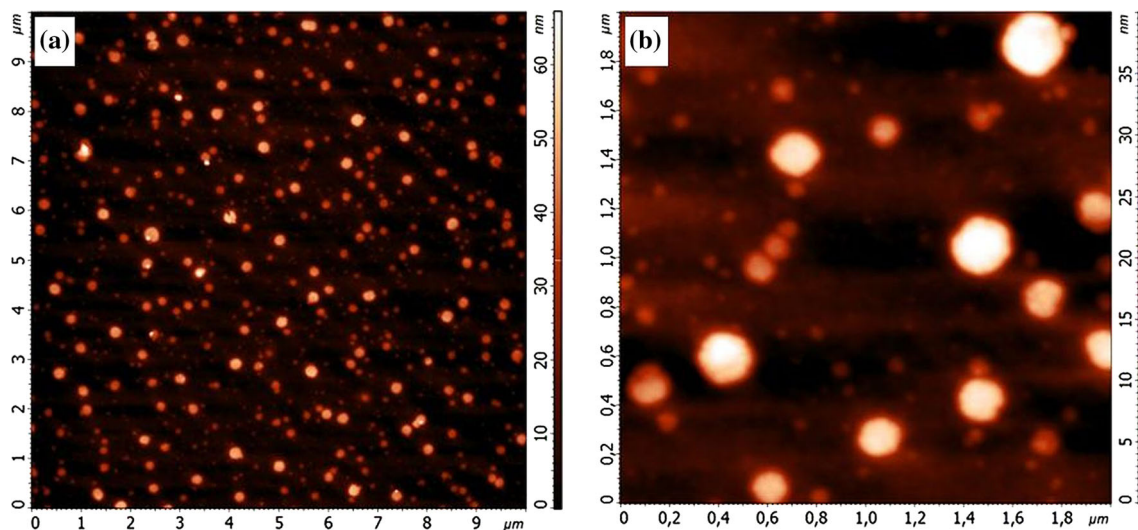


Fig. 7 AFM topological images of PVA/SiO₂/GA3 membrane on **a** micron and **b** submicron scale

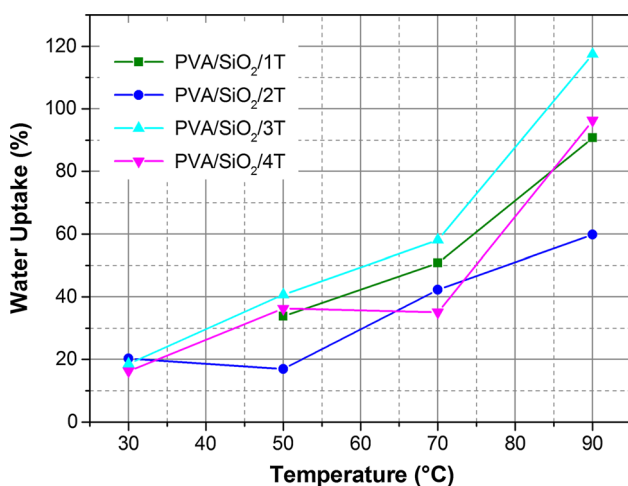


Fig. 8 Water uptake properties of the PVA/SiO₂ membranes

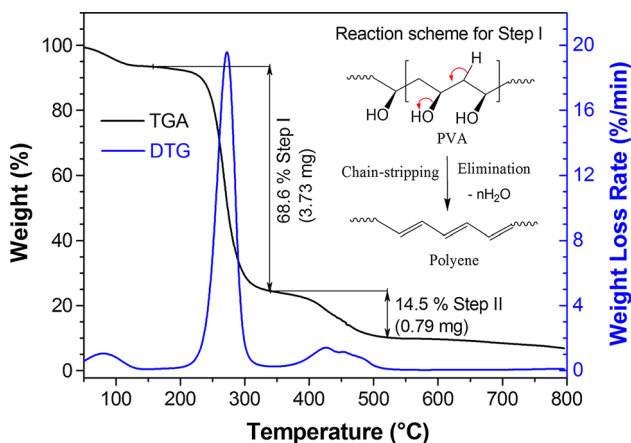


Fig. 9 TGA and DTG curves of pure PVA membrane

easily from the polymer chains in these samples than in the case of pure PVA. This was ascribed to the lower crystallinity going hand in hand with a disturbed regularity of hydrogen bonding in contrast with the regular hydrogen bonding between the PVA chains in the crystallites of pure PVA. The lower crystallinity is caused by the incorporation of small silica nanoparticles which are homogeneously distributed throughout the PVA matrix, as discussed above in the SAXS/WAXS and AFM sections. However, further thermal degradation is slowed down due to the strong chemical bonding between the silica nanoparticles with a high surface area and PVA via its OH groups (see Scheme 1). Some reports also suggested the migration of silica nanoparticles to the surface to form SiO₂/PVA char, which acts as a heating barrier and protects the PVA matrix inside [44, 45]. On the basis of the TGA analyses, it can thus be concluded that the nanoscale deposition of thermally stable silica has effectively enhanced the overall thermal stability of the PVA/SiO₂ membranes.

The difference in the degradation processes of the PVA and PVA/SiO₂ membranes was clearly seen in derivative thermogravimetric (DTG) curves (Fig. 11a). There are two obvious degradation peaks of pure PVA, one sharp peak at 268 °C and a broad peak above 350 °C. The significant change in the shape of the degradation peaks of the PVA/SiO₂ membranes was evident. The main degradation peak of PVA (at 268 °C) was not observed for the PVA/SiO₂ membranes, whereas two minor peaks with lower intensities were observed at ~150 and ~450 °C. In the PVA/SiO₂ membranes, the elimination reaction spans over a wide temperature range and starts sooner, as discussed above. The first peak obviously corresponds to the fast onset of the elimination reactions in the PVA/SiO₂ membranes. However, the second peak, corresponding to the second degradation stage, shifted to higher

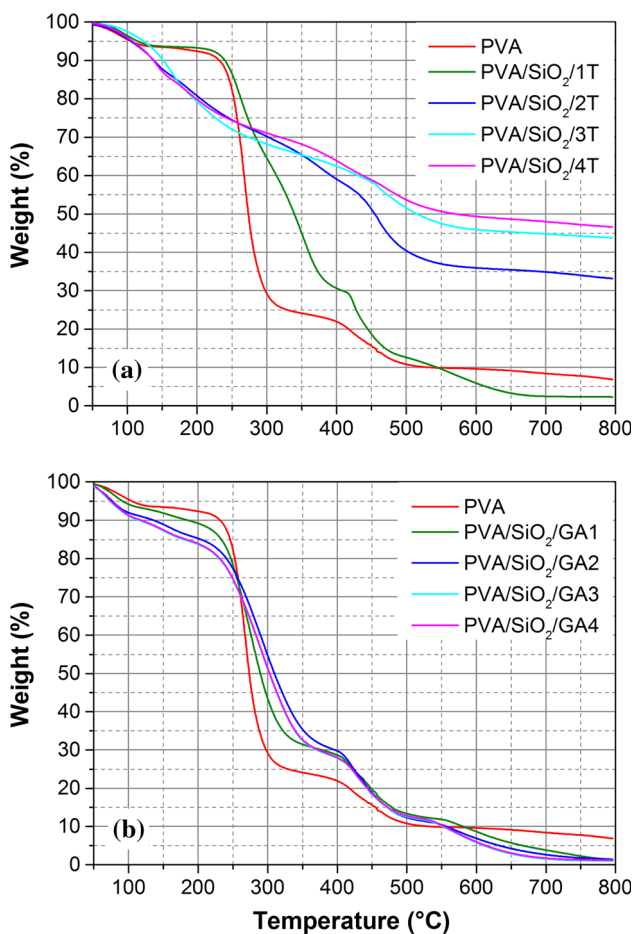


Fig. 10 TGA thermograms of **a** PVA/SiO₂; **b** PVA/SiO₂/GA membranes

temperatures with respect to pure PVA, exhibiting enhancement in the thermal stability. During this stage, the elimination reactions are accompanied by several chain-scission reactions, cyclization, and side reactions. Peng and Kong [44] identified the degradation products as low-molecular weight polyenes, acetaldehyde, benzenoid derivatives, furan, acetone, and acetic acid. It can be observed that the second peak is superimposed on a background originating from the first degradation stage. The overlap of the two stages can be better observed from the integral dependencies (TGA).

The degradation behavior of the PVA/SiO₂/GA membranes was similar to that of the pure PVA membranes (Figs. 10b, 11b). In other words, the incorporation of GA only had a small influence on the membrane thermal stability. The membranes exhibited a weight loss of about 70 % in the first stage (50–350 °C), with a further loss of 25 % in the second stage as shown in Fig. 10b. In this case, GA and TEOS did not bind effectively with the PVA network, which lead to the formation of bigger particles (confirmed by SAXS and AFM) instead of the small nanoparticles formed in the PVA/SiO₂ samples. Therefore,

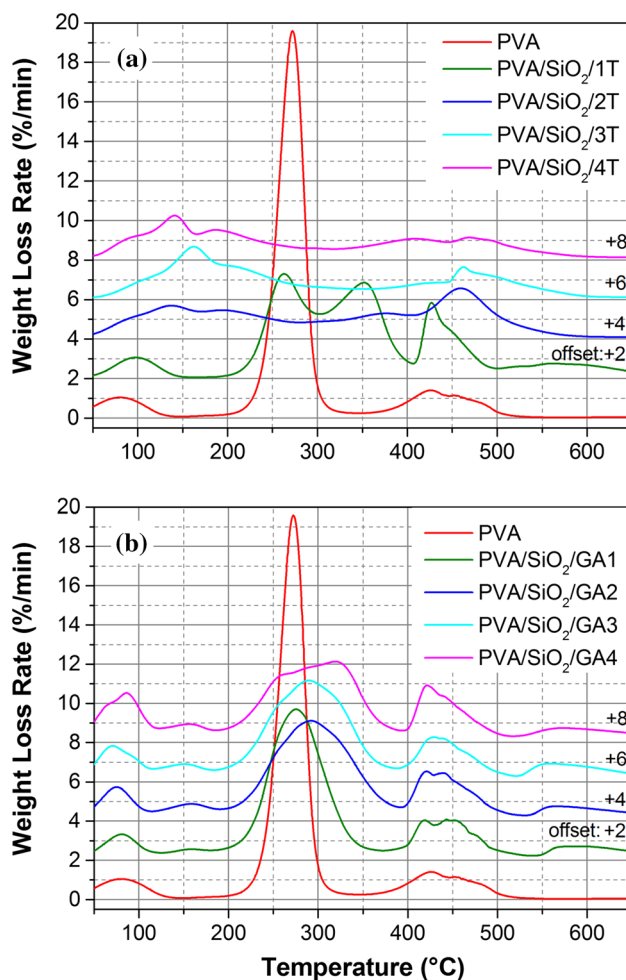


Fig. 11 DTG curves of **a** PVA/SiO₂; **b** PVA/SiO₂/GA membranes

the thermal stability did not increase upon silica addition, contrary to the PVA/SiO₂ membranes.

The only significant change in the TGA curves of PVA/SiO₂/GA compared to pure PVA was the broader first stage of the weight loss corresponding to the elimination reactions. This correlates very well with the decrease in crystallinity of the PVA/SiO₂/GA membranes in comparison with pure PVA, which was proved by WAXS and Raman spectroscopy (see Figs. 2, 4). However, the first weight loss stage of PVA/SiO₂/GA is not that broad as in the case of PVA/SiO₂, which reflects the fact that the crystallinity of the PVA/SiO₂ membranes is lower than that of the corresponding PVA/SiO₂/GA membranes (compare the WAXS spectra in Fig. 4 and the Raman spectra in Fig. 2). Thus, the width of the temperature range of the first decomposition stage reflects very well the crystallinity of the samples: the most crystalline PVA showed the fastest decomposition, followed by the less ordered PVA/SiO₂/GA samples with a slower decomposition, and finally by the most amorphous PVA/SiO₂ samples.

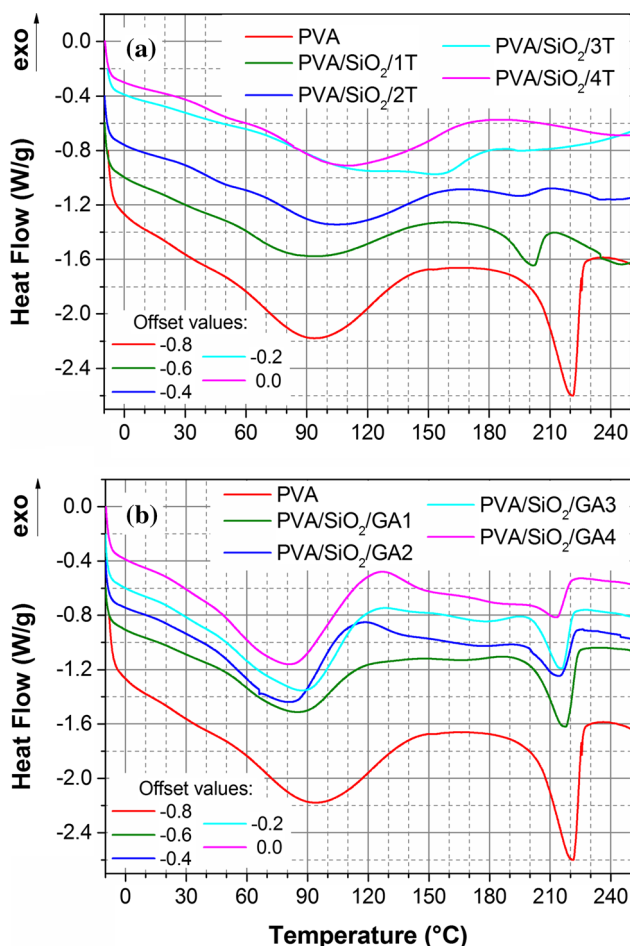


Fig. 12 DSC scans of **a** PVA/SiO₂ and **b** PVA/SiO₂/GA membranes

DSC profiles of PVA and PVA/SiO₂ are shown in Fig. 12a. PVA exhibited a clear melting transition (T_m) at 223 °C, whereas T_m of the PVA/SiO₂ membranes ranged from 176 to 204 °C, i.e., were lower than that of the pure PVA membrane. The melting peaks of the PVA/SiO₂ membranes decreased in intensity and shifted to lower temperatures with increasing silica loading. This decline is clearly seen for PVA/SiO₂/1T, but as the silica loading increases, the endothermic melting peak becomes broader and totally vanishes for the PVA/SiO₂/3T and PVA/SiO₂/4T membranes. Both the decrease of T_m and the broadening of the melting peak can be attributed to the reduced crystallinity due to the incorporated SiO₂ nanoparticles. Bin et al. reported this kind of behavior for PVA–VGCF and PVA–MWNT composites [46].

The DSC profiles of the PVA/SiO₂/GA membranes (Fig. 12b) showed a similar melting transition as the pure PVA membrane with only a small decrease in T_m . This is in agreement with the smaller decrease in crystallinity compared to the PVA/SiO₂ samples. The increase in GA concentration had a relatively small effect on the endothermic

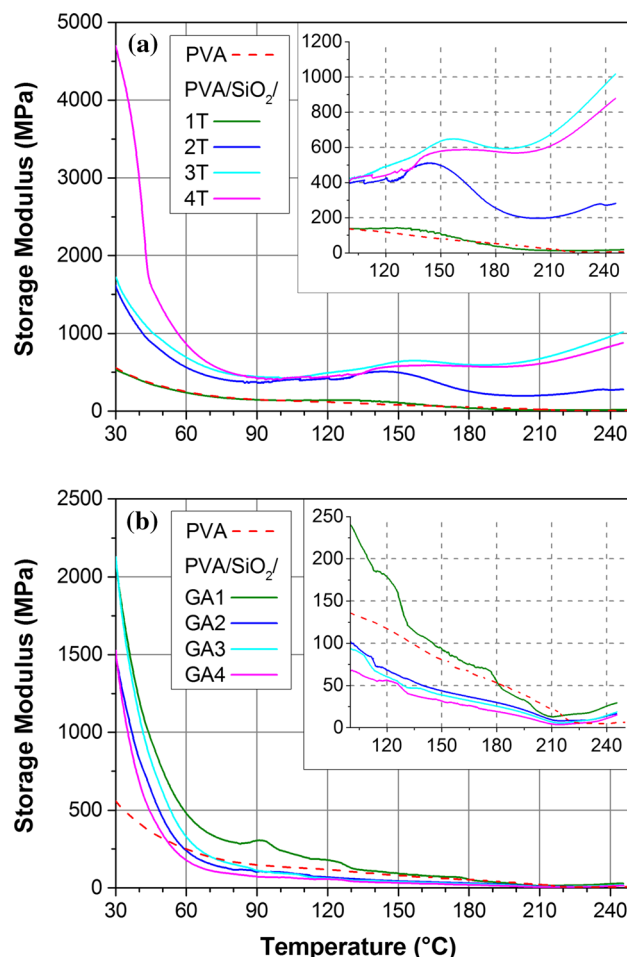


Fig. 13 DMA curves of **a** PVA/SiO₂; **b** PVA/SiO₂/GA membranes

transition of the PVA/SiO₂/GA membranes. This correlates well with the already discussed fact that the influence of GA concentration on the crystallinity of the PVA/SiO₂/GA membranes is not that strong as in the case of the PVA/SiO₂ membranes.

Dynamic mechanical analysis

DMA analysis was performed to investigate the thermo-mechanical properties of the nanocomposite membranes. The temperature dependence of the storage modulus (E') was measured in the range from 30 to 250 °C. At higher temperatures (>200 °C), where the material enters the rubbery phase, the storage modulus is referred to as rubbery modulus, E_R .

In the case of PVA/SiO₂ membranes, E' increased with the increasing silica loading as shown in Fig. 13a. The membranes displayed a higher E' in the initial stages from 30 to 70 °C, followed by a flat mid-region between 70 and 120 °C. A subsequent increase in E' was observed at higher temperatures (>200 °C) for the 2T, 3T, and 4T samples.

The inset graph in Fig. 13a shows a zoom of the plot for higher temperatures, i.e., the dependencies of rubbery modulus, E_R versus temperature for the PVA/SiO₂ membranes. Depending on the silica loading, E_R values ranged from 17 to 1015 MPa at 250 °C. PVA/SiO₂/4T exhibited the highest E_R value of 1015 MPa and PVA/SiO₂/1T displayed the lowest E_R of 17 MPa. The E_R value of pure PVA was 6 MPa at 250 °C. We can thus conclude that the silica loading clearly improved the mechanical strength of the membranes.

On the other hand, the presence of GA has shown an adverse effect on the PVA/SiO₂/GA membrane strength (Fig. 13b). The inset graph in Fig. 13b shows a detail of the plot for higher temperatures. These membranes followed a reverse trend, i.e., the PVA/SiO₂/GA1 membrane exhibited the highest E_R of 28 MPa at 250 °C and the other membranes showed a decrease of E_R with the increasing GA concentration down to 15 MPa in the case of PVA/SiO₂/GA4. This can be explained based on our previous conclusions. In the PVA/SiO₂ membranes, the silica incorporates into the membrane structure in the form of small nanoparticles and binds with the PVA polymer, whereas in the presence of GA, larger separated particles of GA and silica were observed. The presence of these larger nanoparticles resulted in the inferior thermo-mechanical stability of these membranes.

Conclusions

We successfully prepared PVA-based nanocomposite membranes with various silica and GA loading (PVA/SiO₂ and PVA/SiO₂/GA) via the solution casting method. Membranes with and without GA displayed considerably different characteristic features. SAXS/WAXS, AFM and Raman spectroscopy confirmed the incorporation of fine silica nanoparticles (~1 nm) into the PVA/SiO₂ membranes. These membranes showed a significant improvement in the water uptake, thermal stability, and mechanical strength compared to the pure PVA and PVA/SiO₂/GA membranes. The PVA/SiO₂/3T membrane with high silica loading exhibited the best thermo-mechanical stability with E_R of 1015 MPa (at 250 °C, DMA). In the case of PVA/SiO₂/GA membranes, GA preferably reacted with TEOS forming submicron particles (>25 nm) contrary to PVA/SiO₂ membranes, which reduced the thermal stability of these membranes. The comparison of structural and thermo-mechanical characteristics of the PVA/SiO₂ and PVA/SiO₂/GA membranes indicates that the homogeneous incorporation of small silica nanoparticles (~1 nm) played a crucial role in improving the properties of the PVA/SiO₂ membranes. These membranes are both hydrophilic and

thermally stable, which are important criteria for the application of PVA-based membranes. Furthermore, they are produced without any cross-linking agent such as GA, which makes the process simpler and cost-effective.

Acknowledgements The result was developed within the CENTEM project, reg. no. CZ.1.05/2.1.00/03.0088, cofunded by the ERDF as part of the Ministry of Education, Youth and Sports OP RDI programme and, in the follow-up sustainability stage, supported through CENTEM PLUS (LO1402) by financial means from the Ministry of Education, Youth and Sports under the National Sustainability Programme I. Financial support from specific university research (MSMT No 21/2015) is acknowledged. The authors would like to thank to Jan Beneš for careful technical assistance with the measurement of Raman spectra.

References

- Lin W, Zhu T, Li Q, Yi S, Li Y (2012) Study of pervaporation for dehydration of caprolactam through PVA/nano silica composite membranes. *Desalination* 285:39–45
- Ceia TF, Silva AG, Ribeiro CS, Pinto JV, Casimiro MH, Ramos AM, Vital J (2014) PVA composite catalytic membranes for hyacinth flavour synthesis in a pervaporation membrane reactor. *Catal Today* 236:98–107
- Yang D, Li Y, Nie J (2007) Preparation of gelatin/PVA nanofibers and their potential application in controlled release of drugs. *Carbohydr Polym* 69:538–543
- Yadav R, Kandasubramanian B (2013) Egg albumin PVA hybrid membranes for antibacterial application. *Mater Lett* 110:130–133
- Wu Y, Wu C, Li Y, Xu T, Fu Y (2010) PVA–silica anion-exchange hybrid membranes prepared through a copolymer crosslinking agent. *J Membr Sci* 350:322–332
- Chen H, Yuan D, Li Y, Dong M, Chai Z, Kong J, Fu G (2013) Silica nanoparticle supported molecularly imprinted polymer layers with varied degrees of crosslinking for lysozyme recognition. *Anal Chim Acta* 779:82–89
- Liu Z, Dong Y, Men H, Jiang M, Tong J, Zhou J (2012) Post-crosslinking modification of thermoplastic starch/PVA blend films by using sodium hexametaphosphate. *Carbohydr Polym* 89:473–477
- Santos C, Silva CJ, Büttel Z, Guimarães R, Pereira SB, Tamagnini P, Zille A (2014) Preparation and characterization of polysaccharides/PVA blend nanofibrous membranes by electrospinning method. *Carbohydr Polym* 99:584–592
- Li G, Zhao Y, Lv M, Shi Y, Cao D (2013) Super hydrophilic poly(ethylene terephthalate) (PET)/poly(vinylalcohol) (PVA) composite fibrous mats with improved mechanical properties prepared via electrospinning process. *Colloids Surf A* 436:417–424
- Na H, Chen P, Wong SC, Hague S, Li Q (2012) Fabrication of PVDF/PVA microtubules by coaxial electrospinning. *Polymer* 53:2736–2743
- Zhu M, Qian J, Zhao Q, An Q, Li J (2010) Preparation method and pervaporation performance of polyelectrolyte complex/PVA blend membranes for dehydration of isopropanol. *J Membr Sci* 361:182–190
- Irani M, Keshtkar AR, Moosavian MA (2012) Removal of cadmium from aqueous solution using mesoporous PVA/TEOS/APTES composite nanofiber prepared by sol–gel/electrospinning. *Chem Eng J* 200–202:192–201

13. Zeng C, He Y, Li C, Xu Y (2013) Synthesis of nanocrystalline $\text{LaMn}_{0.5}\text{Fe}_{0.5}\text{O}_3$ powders via PVA sol–gel route. *Ceram Int* 39:5765–5769
14. Holloway JL, Lowman AM, Landingham MRV, Palmese GR (2013) Chemical grafting for improved interfacial shear strength in UHMWPE/PVA-hydrogel fiber-based composites used as soft fibrous tissue replacements. *Compos Sci Technol* 85:118–125
15. Aiji Z, Ali AM (2010) Separation of copper ions from iron ions using PVA-g-(acrylic acid/*N*-vinylimidazole) membranes prepared by radiation-induced grafting. *J Hazard Mater* 173:71–74
16. Morgado PI, Lisboa PF, Ribeiro MP, Miguel SP, Simões PC, Correia IJ, Ricardo AA (2014) Poly(vinylalcohol)/chitosan asymmetrical membranes: highly controlled morphology toward the ideal wound dressing. *J Membr Sci* 469:262–271
17. Li N, Xiao C, An S, Hu X (2010) Preparation and properties of PVDF/PVA hollow fiber membranes. *Desalination* 250:530–537
18. M'barki O, Hanafia A, Bouyer D, Faur C, Sescousse R, Delabre U, Blot C, Guenoun P, Deratani A, Quemener D, Pochat-Bohatier C (2014) Greener method to prepare porous polymer membranes by combining thermally induced phase separation and crosslinking of poly(vinyl alcohol) in water. *J Membr Sci* 458:225–235
19. Casimiro MH, Silva AG, Alvarez R, Ferreira LM, Ramos AM, Vital J (2014) PVA supported catalytic membranes obtained by γ -irradiation for biodiesel production. *Radiat Phys Chem* 94:171–175
20. Lai T, Lind ML (2015) Heat treatment driven surface segregation in $\text{Pd}_{77}\text{Ag}_{23}$ membranes and the effect on hydrogen permeability. *Int J Hydrogen Energy* 40:373–382
21. Wu H, Li X, Nie M, Li B, Jiang Z (2011) Integral PVA–PES composite membranes by surface segregation method for pervaporation dehydration of ethanol. *Chin J Chem Eng* 19:855–862
22. Yang CC, Lee YJ, Yang JM (2009) Direct methanol fuel cell (DMFC) based on PVA/MMT composite polymer membranes. *J Power Sources* 188:30–37
23. Keshkar AR, Irani M, Moosavian MA (2013) Comparative study on PVA/silica membrane functionalized with mercapto and amine groups for adsorption of Cu(II) from aqueous solutions. *J Taiwan Inst Chem Eng* 44:279–286
24. Yang CC, Chiu SJ, Kuo SC (2011) Preparation of poly(vinylalcohol)/montmorillonite/poly(styrene sulfonic acid) composite membranes for hydrogen–oxygen polymer electrolyte fuel cells. *Curr Appl Phys* 11:229–237
25. Li X, Chen Y, Hu X, Zhang Y, Hu L (2014) Desalination of dye solution utilizing PVA/PVDF hollow fiber composite membrane modified with TiO_2 nanoparticles. *J Membr Sci* 471:118–129
26. Zhang CH, Yang FL, Wang WJ, Chen B (2008) Preparation and characterization of hydrophilic modification of polypropylene non-woven fabric by dip-coating PVA (polyvinyl alcohol). *Sep Purif Technol* 61:276–286
27. Tong HW, Mutlu BR, Wackett LP, Aksan A (2013) Silica/PVA biocatalytic nanofibers. *Mater Lett* 111:234–237
28. Flynn EJ, Keane DA, Tabari PM, Morris MA (2013) Pervaporation performance enhancement through the incorporation of mesoporous silica spheres into PVA membranes. *Sep Purif Technol* 118:73–80
29. Pandey J, Mir FQ, Shukla A (2014) Synthesis of silica immobilized phosphotungstic acid (Si-PWA)-poly(vinyl alcohol) (PVA) composite ion-exchange membrane for direct methanol fuel cell. *Int J Hydrogen Energy* 39:9473–9481
30. Martinelli A, Matic A, Jacobsson P, Börjesson L, Navarra MA, Fernicola A, Panero S, Scrosati B (2006) Structural analysis of PVA-based proton conducting membranes. *Solid State Ionics* 177:2431–2435
31. Yang CC, Li YJ, Liou TH (2011) Preparation of novel poly(vinyl alcohol)/ SiO_2 nanocomposite membranes by a sol–gel process and their application on alkaline DMFCs. *Desalination* 276:366–372
32. Alessi A, Agnello S, Buscarino G, Gelardi FM (2013) Raman and IR investigation of silica nanoparticles structure. *J Non-Cryst Solids* 362:20–24
33. Yang CC, Lin CT, Chiu SJ (2008) Preparation of the PVA/HAP composite polymer membrane for alkaline DMFC application. *Desalination* 233:137–146
34. Hema M, Selvasekarapandian S, Hirankumar G, Sakunthala A, Arunkumar D, Nithya H (2010) Laser Raman and ac impedance spectroscopic studies of PVA: NH_4NO_3 polymer electrolyte. *Spectrochim Acta A* 75:474–478
35. Assender HE, Windle AH (1998) Crystallinity in poly(vinyl alcohol). 1. An X-ray diffraction study of atactic PVOH. *Polymer* 39:4295–4302
36. Guirguis W, Moselhey MTH (2012) Thermal and structural studies of poly(vinyl alcohol) and hydroxypropyl cellulose blends. *Nat Sci* 4:57–67
37. Hassan CM, Peppas NA (2000) Structure and applications of poly(vinyl alcohol) hydrogels produced by conventional crosslinking or by freezing/thawing methods. *Adv Polym Sci* 153:37–65
38. Ilavsky J, Jemian PR (2009) *Irena*: tool suite for modeling and analysis of small-angle scattering. *J Appl Crystallogr* 42:347–353
39. Mansur HS, Oréfice RL, Mansur AAP (2004) Characterization of poly(vinyl alcohol)/poly(ethylene glycol) hydrogels and PVA-derived hybrids by small-angle X-ray scattering and FTIR spectroscopy. *Polymer* 45:7193–7202
40. Xie Z, Hoang M, Ng D, Doherty C, Hill A, Gray S (2014) Effect of heat treatment on pervaporation separation of aqueous salt solution using hybrid PVA/MA/TEOS membrane. *Sep Purif Technol* 127:10–17
41. Tsuchiya Y, Sumi K (1969) Thermal decomposition products of poly(vinyl alcohol). *J Polym Sci A* 7:3151–3158
42. Gilman JW, Hart DLV, Kashiwagi T (1994) In: Nelson GL (ed) *Fire and polymers II: materials and tests for hazard prevention*. American Chemical Society, Washington, DC, p 161
43. Alexy P, Bakos D, Crkonova G, Kolomaznik K, Krasiak M (2001) Blends of polyvinylalcohol with collagen hydrolysate thermal degradation and processing properties. *Macromol Symp* 170:41–49
44. Peng Z, Kong LX (2007) A thermal degradation mechanism of poly(vinyl alcohol)/silica nanocomposites. *Polym Degrad Stab* 92:1061–1071
45. Vyazovkin S, Sbirrazzuoli N (1999) Kinetic methods to study isothermal and nonisothermal epoxyanhydride cure. *Macromol Chem Phys* 200:2294–2303
46. Bin Y, Mine M, Koganamaru A, Jiang X, Matsuo M (2006) Morphology and mechanical and electrical properties of oriented PVA–VGCF and PVA–MWNT composites. *Polymer* 47:1308–1317